buildings

MDPI

Article

Assessment of Web Panel Zone in Built-up Box Columns Subjected to Bidirectional Cyclic Loads

Ramón Mata [1], Eduardo Nuñez [1,*], Frank Sanhueza [1], Nelson Maureira [1] and Ángel Roco [2,*]

1 Department of Civil Engineering, Universidad Católica de La Santísima Concepción, Concepción 4090541, Chile
2 Facultad de Salud y Ciencias Sociales, Universidad de las Américas, Providencia, Santiago 7500975, Chile
* Correspondence: enunez@ucsc.cl (E.N.); aroco@udla.cl (Á.R.)

Abstract: The behavior of the web panel zone has a direct effect on the cyclic performance of steel moment connections. While the mechanisms of web panel zone failure are known under cyclic load, little is known about the behavior of the web panel zone under bidirectional loads in bolted connections. Using experimental tests and calibrated numerical models, this research evaluated the web panel zone behavior under unidirectional and bidirectional cyclic loads. The results showed that bidirectional load can modify the stress and strain distribution in the web panel zone. Moreover, the increasing of the width-to-thickness ratio of the column influences the failure mechanism of the joint configuration and increases the plastic incursion in the column. These data demonstrate that bidirectional effects improve the web panel zone performance under cyclic loads.

Keywords: web panel zone; cyclic behavior; tubular columns; finite elements; bidirectional load

check for updates

Citation: Mata, R.; Nuñez, E.; Sanhueza, F.; Maureira, N.; Roco, Á. Assessment of Web Panel Zone in Built-up Box Columns Subjected to Bidirectional Cyclic Loads. *Buildings* **2023**, *13*, 71. https://doi.org/10.3390/buildings13010071

Academic Editors: Chiara Bedon, Flavio Stochino, Mislav Stepinac and Binsheng (Ben) Zhang

Received: 21 October 2022
Revised: 12 December 2022
Accepted: 15 December 2022
Published: 28 December 2022

1. Introduction

The seismic provisions in [1] establish requirements for the use of moment-resisting frames in high-risk seismic zones to avoid brittle failure mechanisms. Within these requirements, the use of prequalified moment connections according to [2] is necessary to guarantee the dissipation of energy from the structure because of the inelastic bending incursion of the beam. All these connections are designed to avoid damage to the column, the welding fracture or shear yielding in the web panel zone (WPZ). If the WPZ is weak in shear, the joint will be a weak link with plastic deformations, while the beams will not develop their flexural resistance under cyclic loading, reducing the strength and stiffness of the structure significantly [3].

The investigation conducted by [4] assessed the deformation demands on the WPZ of steel moment frames through a parametric analysis using numerical models and design requirements for AISC 360 [5], FEMA-355D [6], and Eurocode 3 [7]. The results found that the research in [6] provides lower capacity and less inelastic incursion than [5,7], which present similar capacities. Similarly, the research developed in [8] proposed a numerical model for beam-to-column connections with the inelastic behavior of the WPZ in moment frames being verified through nonlinear static and dynamic analyses. The results show an increase in inelastic response and energy dissipation capacity with lower maximum structure strength without indication of a soft-story collapse mechanism in the range of deformation under 15 times the panel yield deformation. Nevertheless, this research considers a uniaxial bending effect on the panel zone and higher levels of inelastic deformation than the studies.

On the other hand, [9] shows the importance of the WPZ strength in slotted-web beam connections through a combined numerical and experimental study. The results show that high participation of the panel zone effect causes weld fracture in the beam web and decreases the connection. In this sense, several studies [10–13] have evaluated the strength and performance of the panel zone, noting that both short and long web panels have substantial post-buckling capacities. Furthermore, when the panel zone is subjected to extremely large inelastic demands, this could cause a potential material fracture and thus brittle failure in the column. Further research developed in [14] analyzed the behavior of corrugated web panel zones, obtaining a limited influence of the corrugated forms in the connection shear strength. In addition, the corrugated panels achieved a residual strength of 50% the buckling shear strength; therefore, the use of residual capacity in the design to prevent brittle failure was recommended.

To improve the behavior of the panel zone, intermediate and panel stiffeners are attached to the plate girder web panel to increase the shear strength or reduce the panel aspect ratio to limit the local buckling. The research conducted in [15] proposed a design procedure for intermediate transverse stiffeners through a set of design equations to predict the post-buckling shear strength, emphasizing the necessity of transverse stiffeners specially when the panel aspect ratio is greater than 1.0. On the other hand, [16] experimentally evaluated the effect of these stiffeners on the WPZ shear stability on cruciform beam-to-column connections. The results showed a decrease of the shear buckling in the WPZ and hysteresis behavior improved.

Based on these results, several steel moment connections have been proposed, including stiffeners in their configurations to improve the panel zone performance in investigations developed in [17–24]. Specifically, in the research conducted in [25], different joint assemblies of a new welded moment connection with horizontal stiffeners and tubular columns were performed to estimate their bidirectional cyclic behavior. An important reduction in terms of shear and bending was reached in the column. Moreover, higher deformation of the WPZ was correctly distributed by the internal diaphragm. Likewise, the study developed in [26] assessed the WPZ shear strength in cruciform columns and box columns with continuity plates using the finite element method (FEM). The results showed that cruciform sections have similar plastic capacities to box sections and more shear strength in the WPZ.

More specifically, the experimental research conducted in [27] studied steel tube panels under lateral cyclic load and focused on the evaluation of stiffness and dissipated energy on each cycle of loading. The tubes were tested as boundary elements of the shear wall had local buckling close to the base due to high compression forces and fracture near the top close to the beam. In addition, the behavior of the tubes was similar to a cantilever beam with a hysteretic behavior that showed a slight pinching without stiffness and strength degradations. Furthermore, the research conducted in [28] evaluated experimentally, numerically, and analytically the shear behavior of the panel zone in connection to hollow structural section columns (HSS) in the plane. The results reveal that for this connection, the main failure mode was a shear failure in the plane zone where shear deformation and local buckling occur. The hysteretic behavior exhibited good ductility and stability, showing that an increasing thickness of the tube increases the ultimate shear resistance.

However, this research does not evaluate the behavior under bidirectional cyclic behavior, which is a limitation in assessing the behavior of 3D joints. In this sense, the research conducted in [23] studies the seismic behavior of steel beam-column joint connections with outer stiffeners and welding connections under bidirectional cyclic loads. The prototypes were HSS columns with welded connections to annular stiffeners and beams, which presented inward buckling of the column and fracture of the ring stiffener during the test. In addition, the bidirectional cyclic load reduced the strength connection capacity compared to unidirectional loading. Finally, a stress concentration occurs along the diagonal line of HSS columns in 3D joints with a possibility of brittle failure if the outer annular stiffener is not present. Nevertheless, this research did not contemplate the use of a bolted connection to prevent brittle failure as a fracture or local buckling in the column.

On the other hand, as the number of prequalified connections is limited and most of them are used for wide-flange columns, there was a need for a new proposal for tubular connections. In addition, the implementation of tubular columns brings some limitations due to their commercial availability, which commonly does not have sufficient thickness to comply with seismic limitations for use in special and intermediate moment frames. One of these proposals is the connection developed in [22], which demonstrates experimental and numerical compliance with the requirements of [1,2] without the presence of brittle failures. However, this study did not evaluate the behavior of the proposed connection under bidirectional loads. In this sense, two numerical studies, [29,30], allow us to evaluate the behavior of the mentioned connection under bidirectional cyclic loads and axial loading for five connection configurations. The results of these investigations showed that the axial load was not critical for the connection and the damage was limited to beams in the joint configurations subjected to bidirectional cyclic loads. Nevertheless, these studies were limited in terms of configurations and the sizes of the specimens; therefore, propagation of the results to other configurations is not recommended.

In this context, an extensive parametric study was developed by [31] analyzing the effects of different column sizes, the number of beams, clear span-to-depth beam ratio (L/d), and axial load parameters on cyclic behavior using numerical models in FE. The results showed that all configurations analyzed conformed to the criteria established in [1], even for L/d ratios in the range between 7–20. In addition, the assemblies designed with low axial load are controlled by the design of the WPZ shear, while high levels are controlled by the strong column–weak beam relationship.

All these studies ensure that the connection proposed in [22] has a successful performance for every configuration even under bidirectional loads. However, these numerical studies calibrated their models from unidirectional cyclic tests and do not assess the web panel zone behavior in the column, which can control the joint design.

The aim of this research is the assess the cyclic behavior of the web panel zone in built-up box columns using moment connection subjected to bidirectional load. In this sense, the cyclic response is characterized through the full-scale experimental tests and extended to different sizes using numerical models calibrated from experimental data. Two experimental tests of the joints subjected to unidirectional plane and bidirectional cyclic loads are performed to compare the cyclic behavior. In addition, six numerical models were validated and calibrated with the results of the experimental program, allowing to extrapolate the study to other scenarios untested experimentally. Finally, conclusions are presented in reference to the web panel zone shear behavior and its influence on the hysteretic responses of the joints, which are not commonly evaluated using bidirectional moment connections.

2. Experimental Study

2.1. Test Specimens

Experimental tests on two specimens subjected to pseudo-static cyclic loading were performed. In Figure 1, the setup of specimens and joint assembly tested are shown. The assembly of specimens are based on a prequalification test according to Chapter K [1], applying the cyclic load to capture the bidirectional effect at the top of the column according to [31]. The joint studied consisted of I-beams connected to the built-up box column through the end-plate moment connection proposed in [22], using outer stiffeners and A325 bolts. To consider the bidirectional effect, interior joint configuration with two beams in the plane (2BI) and exterior joint configuration with two beams in corner position (2BC) were tested. Beams and columns satisfy the requirements established in [1] for high-ductility members. The beams and columns were designed to comply with the design requirements of [1,2], resulting in a 220 mm $\times$ 220 mm $\times$ 14 mm square built-up box column and IPE-200 beam. The end-plate thickness, bolts, and outer stiffener are shown in Figure 1. A bolt pretension was applied in bolts using a calibrated torque wrench to achieve a 70% load pretension according to [5].

To prevent displacement outside of the plane loaded, lateral restrictions are imposed at the center of the beams and the top of the column. In this study, the length of the column used is 2562 mm, while the length of the beam was estimated at 1315 mm.

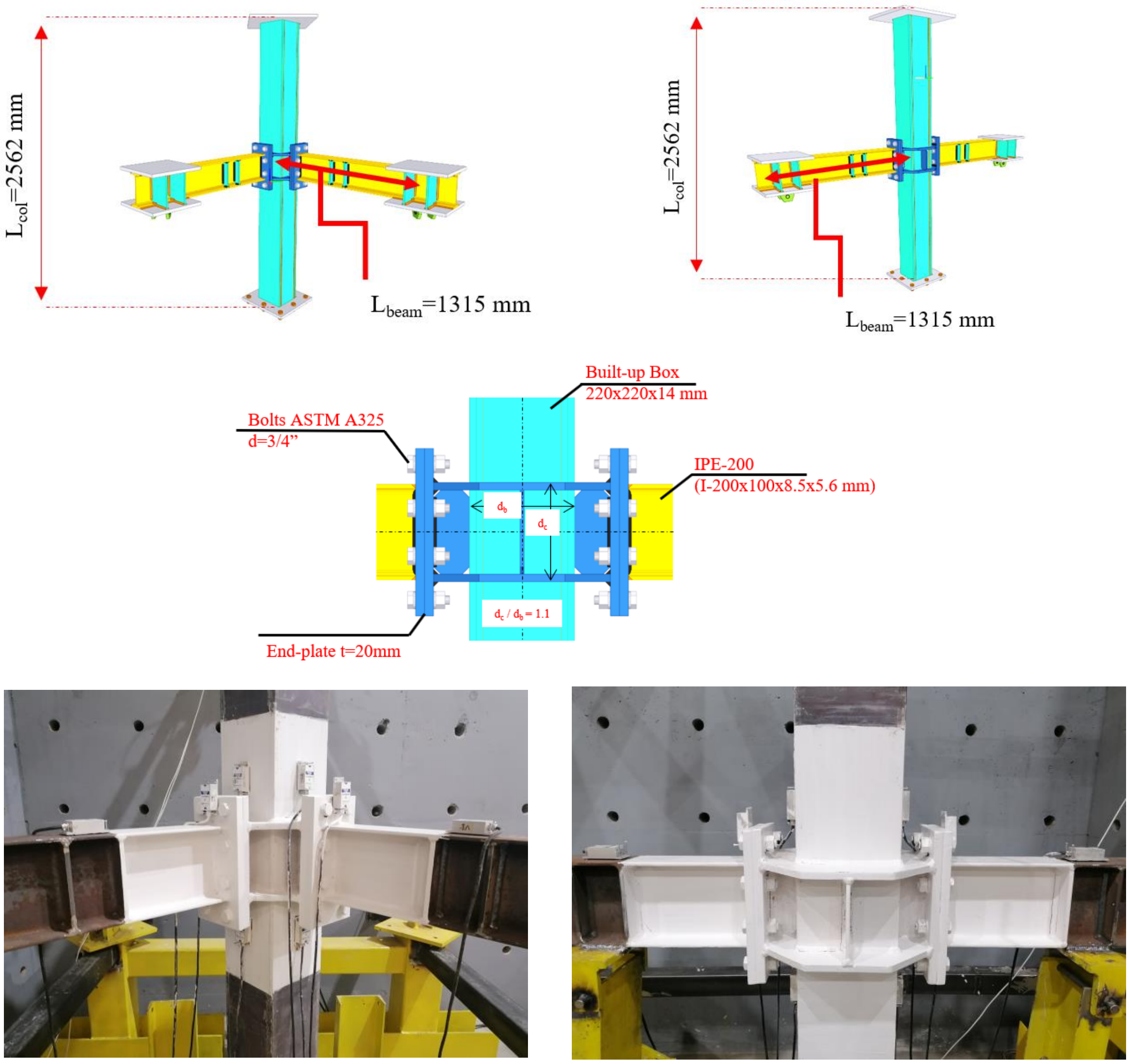

Figure 1. Test assemblies and geometries of the specimens.

2.2. Material Properties

In Table 1, the material properties obtained from the coupon tests are shown. The yield strength (Fy), tensile strength (Fu), and Young's modulus (E) of steel for beam, column, and bolts are reported. A view of the coupon steel tested is shown in Figure 2.

Table 1. Material properties of steel.

Element	Steel Type	Yield Stress (MPa)	Ultimate Stress (MPa)
Beam flange	A36	351	454
Beam flange	A36	349	432
Beam flange	A36	347	439
Beam web	A36	307	403
Beam web	A36	332	407
Beam web	A36	322	410
Column wall	A572 Gr.50	354	550
Column wall	A572 Gr.50	512	575
Column wall	A572 Gr.50	393	559
Bolt	A325	607	801
Bolt	A325	625	814
Bolt	A325	612	807

Figure 2. Test of steel plates samples.

2.3. Test Setup and Loading Procedure

The experimental setup for the cycle load is shown in Figure 3. All specimens were tested using a hydraulic testing machine with a capacity of 25 tons and a stroke of ±130 mm. The velocity of the load application used in the test reached a maximum of 20 mm/min to avoid the presence of inertial forces during the test. The horizontal displacement applied was measured by a linear variable displacement transducer (LVDT) installed between the top of the column and the actuator. The applied load was measured by a load cell in the actuator and the reaction of the beams was measured similarly using a 10-ton capacity load cell. A loading protocol was employed according to the established method in Chapter K of seismic provisions [1].

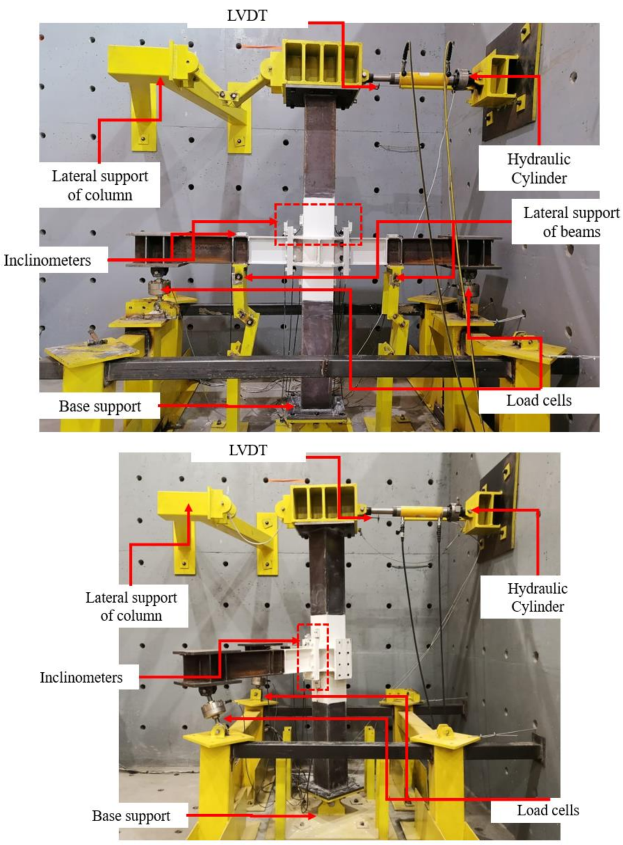

Figure 3. Experimental setup.

2.4. Experimental Results and Discussion

In this section, the results of the experimental program are presented in terms of failure mechanism, hysteretic behavior, dissipation capacity, and stiffness. The key parameters of the tests are shown in Table 2.

Table 2. Summary of the parameters obtained in the experimental tests.

Test #	Ko_West_Beam (kN/rad)	Dissipated Energy (kJ)	Mmax/Mp	θmax (rad)
1 (2BC)	2935	416	1.08	0.04
2 (2BI)	7153	722	1.55	0.04

As shown in Table 2, the dissipated energy is greater in the 2BI specimen in comparison to the 2BC specimen. Therefore, the bidirectional effect reduces the capacity of energy dissipation in steel joint configuration. In Figure 4, the failure modes are shown for the specimen tested. As is expected according to seismic design, the plastic hinges were concentrated in beams, which is required by [1]. Moreover, no failures were reported in the connection components.

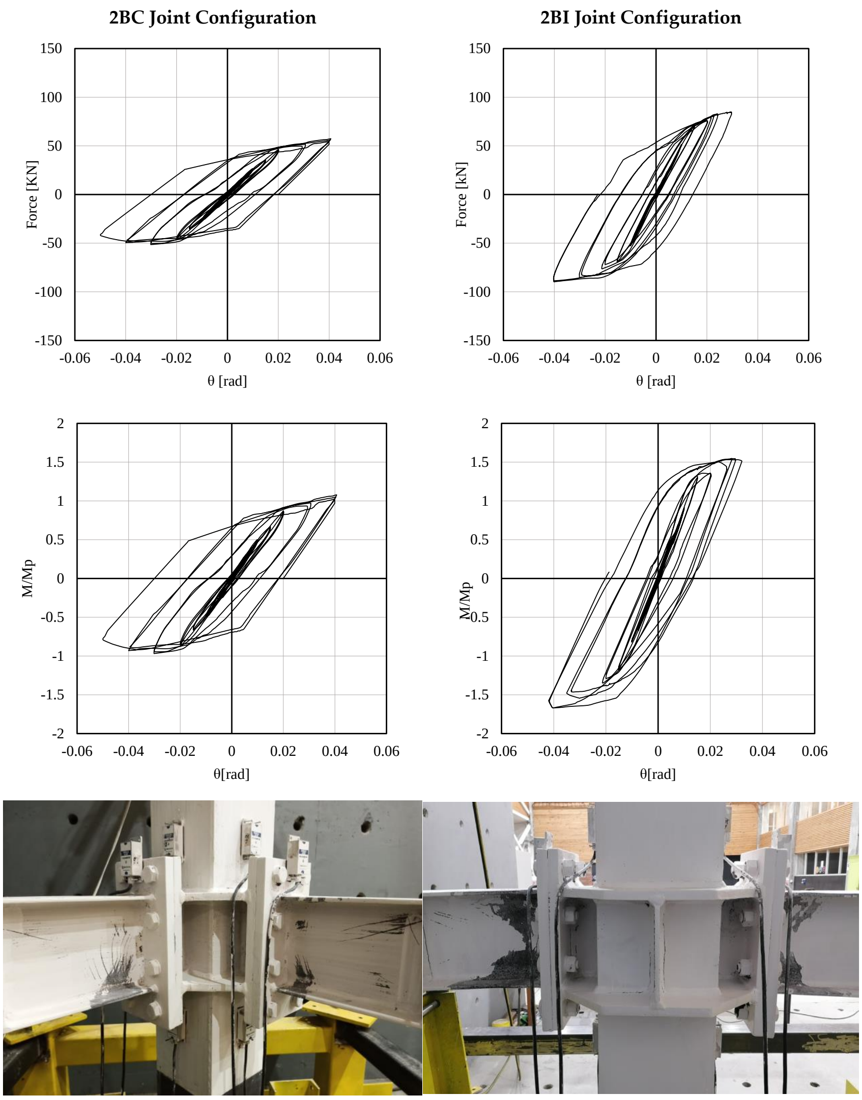

Figure 4. Force-rotation curves and normalized moment-rotation curves of beam and failure mechanisms at 0.04 rad of the specimens tested.

A ductile behavior was exhibited by all specimens tested. However, comparing both joint configurations, greater degradations in the stiffness and strength were observed in 2BC joint in comparison to 2BI joint. Finally, the developed test allows us to verify that the connection proposed in [22] has a successful performance under cyclic loads, complying with the requirements of prequalified moment connections mentioned in [2], and ensuring a ductile failure mechanism without failure in the connection components.

3. Numerical Modeling

The numerical models were developed using the finite element method through the ANSYS software [32]. The original geometry of the tests was considered with the goal to reproduce the configurations tested in the experimental program and extrapolating them to two additional scenarios. The elements and components were modeled explicitly. Loading, constitutive laws of materials, mesh size, and boundary conditions were used to resolve the nonlinear behavior of joints studied. The nonlinearities were considered by means of sub-steps in each load step using the incremental Newton–Raphson method. According to the convergence criterion [32], the convergence force and residual force obtained out of equilibrium must be below the convergence values. Furthermore, the augmented Lagrange method was used to achieve a numerical convergence, according to the investigation carried out in [33].

In the numerical models, the following assumptions were established: the length of the column is considered as the distance between the points of zero moment for each case (the points of zero moment in the columns are assumed to be at half height). The welds are excluded from the model because inelastic incursion is not expected in these elements. The diameters of the holes are estimated as standard holes according to the requirements established in [5]. Additionally, the axial load was not established as its effect was not contemplated in the experimental program. These considerations were verified and employed in [22,29,31].

Numerical models calibrated from the experimental tests were extended to evaluate the cyclic performance of columns with moderate ductility members according to [1]. Moreover, built-up box columns with slender walls according to [5] were studied to evaluate the performance of the WPZ shear. Table 3 shows the dimensions of the elements considered in the numerical model.

Table 3. Geometrical dimensions of the models.

Models	Axial Load (Py)	Configuration	Beam	Column	End-Plate Thickness (mm)	Outer Stiffener Thickness (mm)
Mod-00	0%	2BI	IPE-200	Box 220 × 220 × 14	20	16
Mod-01		2BI	IPE-200	Box 220 × 220 × 9	20	16
Mod-02		2BI	IPE-200	Box 220 × 220 × 4	20	16
Mod-03	0%	2BC	IPE-200	Box 220 × 220 × 14	20	16
Mod-04		2BC	IPE-200	Box 220 × 220 × 9	20	16
Mod-05		2BC	IPE-200	Box 220 × 220 × 4	20	16

3.1. Constitutive Laws of Materials

The constitutive law was considered by means of a bilinear kinematic law and a von Mises yield criterion was used; therefore, no variations in magnitude and location of the yield surface are established. The constitutive law of material was considered from steel coupon tests reported in Section 2. Average values were used to consider the constitutive law according to [34]. For example, in Beam elements, the Young´s modulus, E = 211,908 MPa, yielding stress σy = 334 MPa, and maximum stress σu = 424 MPa were used. The Young´s modulus, E = 196,696 MPa, yielding stress σy = 419 MPa, and maximum stress σu = 561 MPa were considered for square built-up box column elements. In addition, for the bolts, a Young´s modulus, E = 210,625 MPa, yielding stress σy = 615 MPa, and maximum stress σu = 808 MPa were used. The material for the beam is assumed for end plates and horizontal and vertical diaphragms. Posteriorly, the material properties were transformed to true stress and strain values for their use in FE models.

3.2. Boundary Conditions and Loading

To allow for rotation in the base of the column, a pinned restraint was used at the base. The ends of the beams were established as simply supported, with limited movements in Z direction. Moreover, lateral supports to the beam were applied to comply with the stability bracing members of beams according to [1,5]. The loading was applied at the top of the column for the models studied through lateral displacements. Additionally, instability by displacements out of the plane was solved by incorporating lateral support at the top of the column. In Figure 5, support conditions used in the configuration of the two beams corner (2BC) model are shown. A pretension equivalent to 70% of the bolt tension resistance was applied according to [5] to reproduce the real conditions between the plates (see Figure 6).

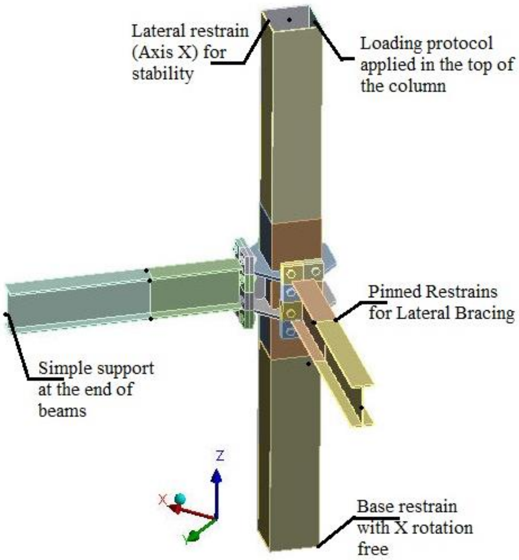

Figure 5. Boundary conditions used in the numerical model.

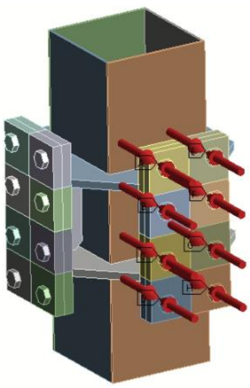

Figure 6. Bolt pretension used in the numerical models.

3.3. Mesh and Element Type

In this study, SOLID 186 elements were employed to simulate all elements. The element is defined by 20 nodes with 3 degrees of freedom per node given from translations in the x, y, and z directions. This element is ideal to model the plasticity, hyperelasticity, creep, stress stiffening, large deflection, and large strain capability, which accurately represent the expected stresses and deformations.

Different mesh sizes have been used to provide accurate results without great computational efforts. In this sense, the inelastic behavior in plastic hinge zones was modeled using a fine mesh, while in other zones, an expected elastic behavior was modeled as a coarser mesh. Furthermore, a sensitivity analysis was performed to obtain the accuracy of the developed model and its convergence with mesh refinement, varying the mesh element's size in the range of 5 mm to 40 mm. Finally, a maximum element size of 5 mm was selected for elements with expected nonlinear behavior, together with 25 mm for those with linear behavior, obtaining a better computational efficiency.

The FEM solves the nonlinear equations using the Newton–Raphson method. Posteriorly, the number of equations is obtained from the number of structure degrees of freedom. Different meshes, sizes, and forms have been used to determine a rational mesh to improve the computational cost. Therefore, the solution adopted uses a fine mesh in zones of interest as high stress or strain regions, specifically in the central zone of the node where the inelastic response is expected, and a coarser mesh in the other regions, as shown in Figure 7.

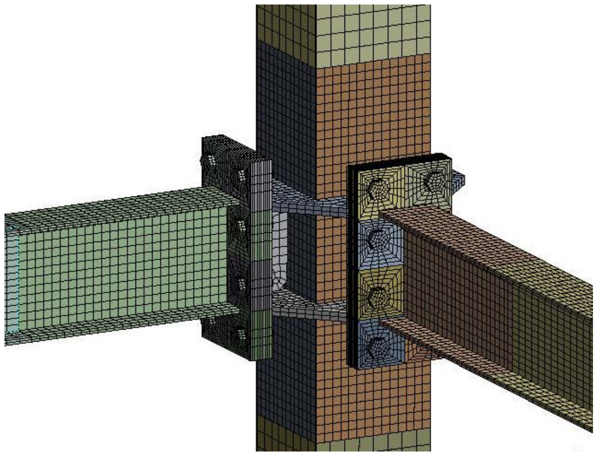

Figure 7. Meshing used in the numerical models.

Additionally, geometrical imperfections were considered according to the geometrical limits established in [35,36]. However, a limited effect of the imperfections on cyclic behavior was obtained. More investigations on these effects and their consequences in the connections can be found in [37].

3.4. Type of Contacts

In this research, a "Bonded" contact was employed to simulate welding conditions and restrained contact in all directions. The contact between the end-plates was considered through "frictional" contact to allow relative displacements between them. A friction coefficient equal to 0.3 was established according to [22]. Trial and error was performed to obtain this value [29,30]. A schematic view of contacts in the joint is shown in Figure 8. Moreover, the type of contact by region is reported in Table 4.

Table 4. Contacts simulated by using elements.

N°	Contact between Elements	Type of Contact
1	End-plates	Frictional (μ = 0.3)
2	Bolt shank in contact to end-plate	
3	Bolt head in contact to end-plate	
4	Nut in contact to end-plate	

Table 4. *Cont.*

N°	Contact between Elements	Type of Contact
5	End-plate in contact to horizontal and vertical stiffener	Bonded
6	Horizontal stiffener in contact to vertical stiffener	
7	Stiffeners in contact to column	
8	End-plate in contact to beam	
9	Bolt shank in contact to bolt head	
10	Bolt shank in contact to nut	
11	Bolt shank in contact to bolt head	
12	Beam in contact to beam	

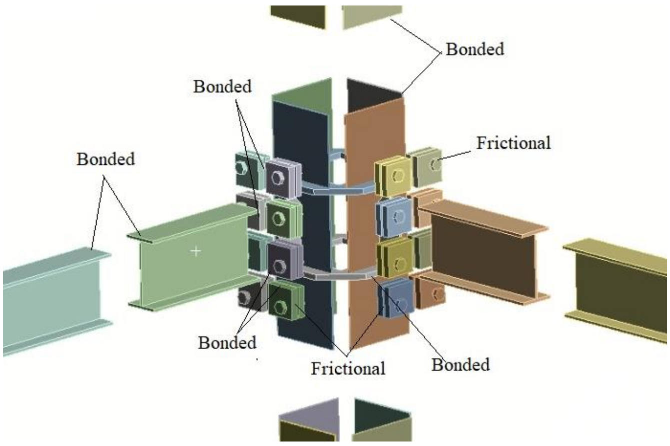

Figure 8. Schematic view of the contacts employed.

3.5. Validation of FEM

Both typologies (2BI and 2BC) of the numerical models were calibrated from the experimental program. The hysteresis curves between the experimental test and FE model were compared. In Figure 9, an acceptable match of curves was obtained; however, slight differences in terms of strength were also obtained. The differences reported may be due to higher overstrength of material in some uncharacterized components. It is important to note that material characterization is performed on limited zones of the components but not on all components.

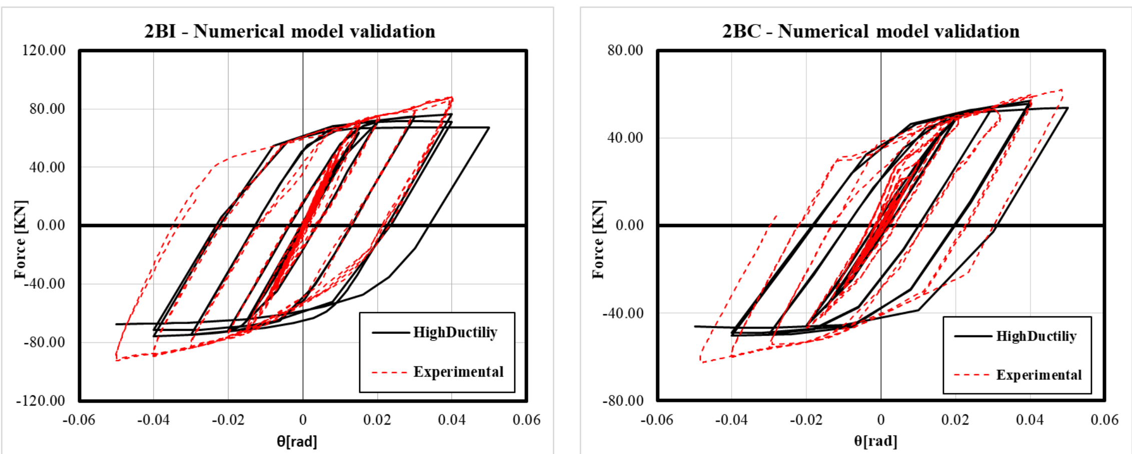

Figure 9. Comparison of the hysteresis curves of the FEM and experimental results.

4. Results

4.1. Stress Distribution

The analysis of the models described in the previous sections displays an equivalent von Mises stress distribution in Figures 10 and 11. These distributions for the different width-to-thickness column ratios show how the stresses increase as the width-to-thickness column ratio decreases.

Model	Front View	Posterior View
High-ductility column		
Moderate-ductility column		
Slender column		

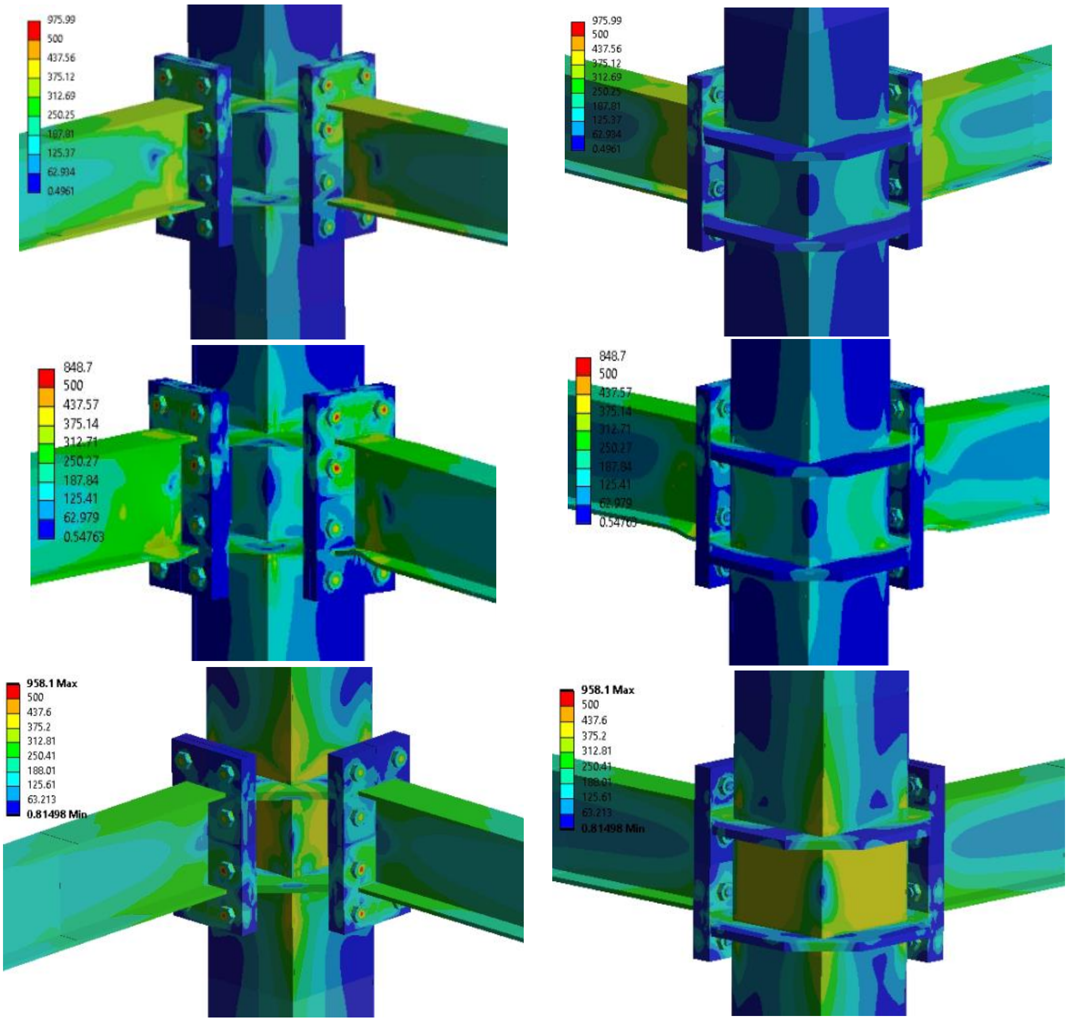

Figure 10. Stress distribution in the 2BC models (Units: MPa).

For 2BC models, the distributions of the stresses are mainly uniform in the web panel zone shear with an increase in the outer annular stiffener as the width-to-thickness column ratio decreases. In addition, the beams are less stressed when the stresses increase in the web panel zone. This demonstrates how the failure mechanism of the connection changes in the zones where the stresses exceed the yielding stress (Fy). Furthermore, the stress distribution in the panel zone is concentrated in the central area, decreasing as it approaches the edges of the column.

For the 2BI models, high-ductility models show a uniform stress distribution concentrated in the center of the web panel zone with a slight concentration in the union of the column with the outer annular stiffener as shown in Figure 11. On the other hand, the moderate-ductility model exhibited an increase in stress in all web panel zones with points of stress concentration in the column outside the web panel zone without exceeding Fy. Likewise, the slender column model shows a stress distribution similar to a tension field action in the panel zone, yielding in shear with values up to Fy. Furthermore, a stress concentration is present in the union of the column with the outer annular stiffener and column edges. Finally, in these 2BI models, the stress distribution in the web panel zone changes from a uniform normal stress distribution to a diagonal shear distribution as the width-to-thickness column ratio increases.

Model **Front View**

High-ductility column

Moderate-ductility column

Slender column

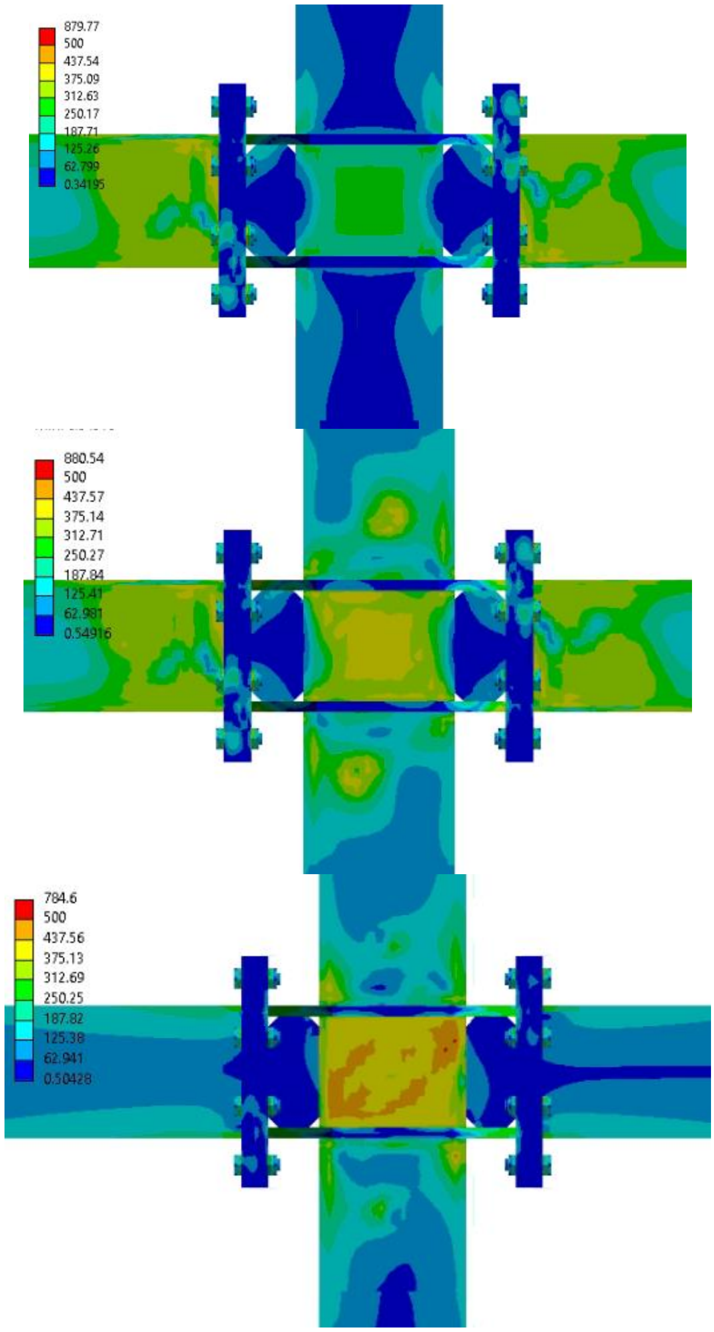

Figure 11. Stress distribution in the 2BI models (Units: MPa).

The comparison of stress distributions between the 2BI and 2BC models demonstrates that when a joint is loaded bidirectionally, the distribution of stresses becomes more uniform. This is translated to a global yielding mechanism for the entire area of the web panel zone if it occurs, contrary to the 2BI case where the shear stresses in the web panel predominate.

4.2. Plastic Strain Distributions

Similar to the previous section, equivalent plastic strains were obtained for all models analyzed and are shown in Figures 12 and 13 for 2BC and 2BI models, respectively. The plastic strain distributions for all high-ductility models show failure mechanisms as plastic hinges at the beams starting from the web yielding to the flange yielding. On the other hand, for moderate-ductility models, plastic hinges are present at the beams. However, a slightly inelastic incursion is shown in the union of the column with the outer annular stiffener and column edges for 2BC models and in the web panel zone for 2BI models.

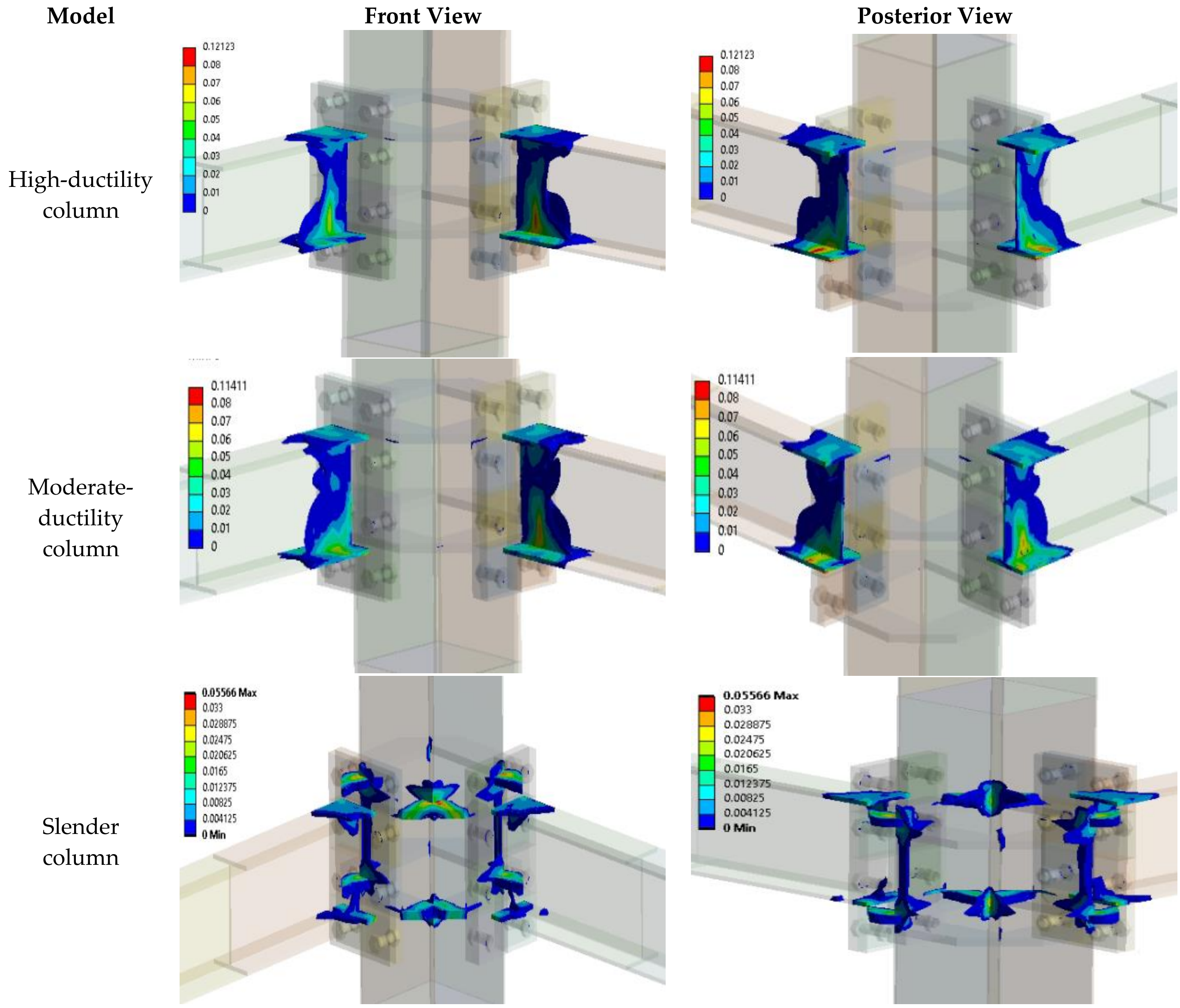

Figure 12. Plastic strain distributions in the 2BC models (Units: mm/mm).

The 2BC slender column model shows an inelastic incursion meaningfully concentrated in the outer annular stiffeners and its union with the column. However, a slight plastic strain appears in the flange of the beams instead of the failure mechanism controlled by the outer annular stiffeners. These stiffeners were designed to the maximum-concentrated beam flange force and had sufficient thickness to avoid high damage in the column and panel zones where plastic strain is not present.

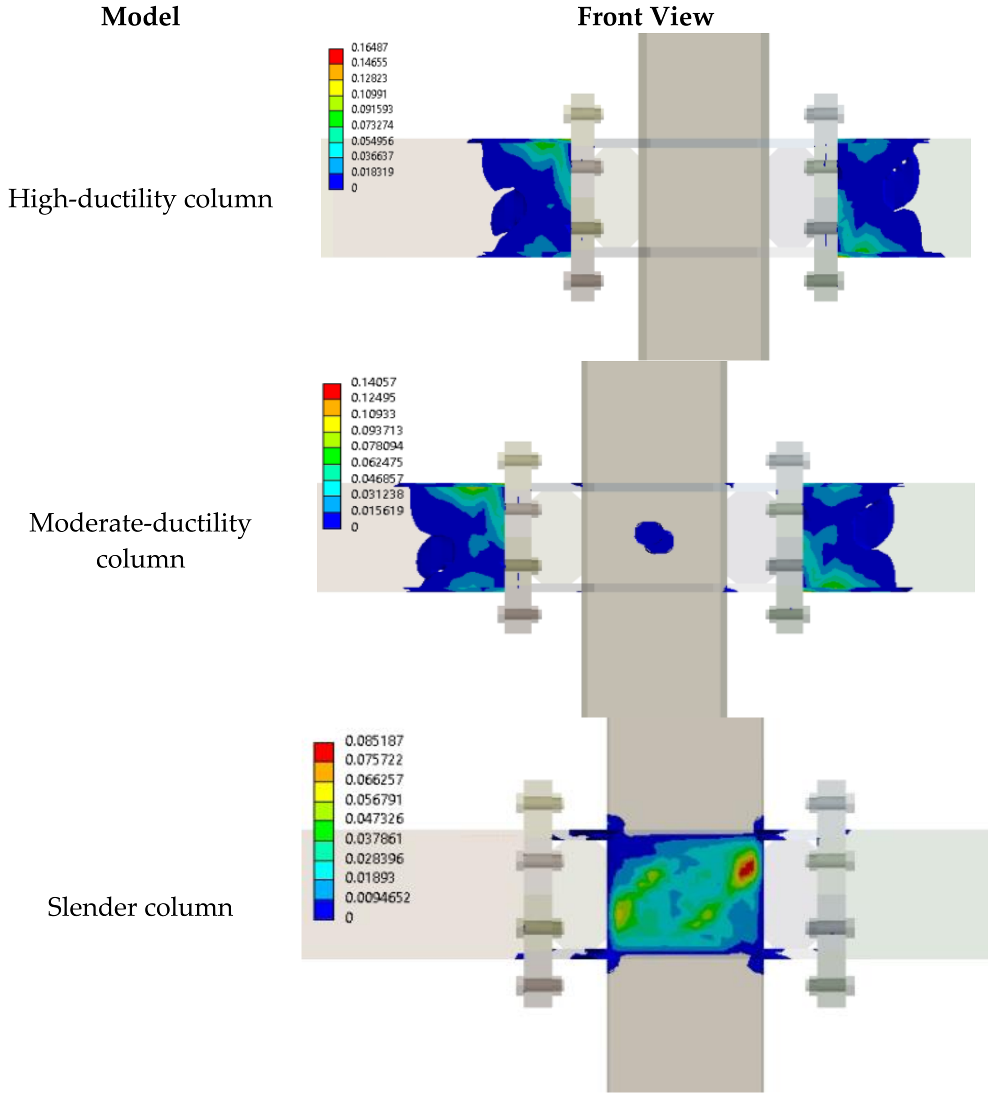

Figure 13. Plastic strain distributions in the 2BI models (Units: mm/mm).

The results of the 2BI slender model show how the plastic strains are concentrated in the web panel zone inducing the shear yielding. Likewise, slight plastic incursion is present in the outer annular stiffeners and in the zone outside the web panel zone. In addition, the strain distribution shows how inelastic behavior starts from the column edges and extends diagonally through an edge-to-edge diagonal stress field. Finally, for all high-ductility models, higher plastic strains are present in comparison to the configurations of other models. Likewise, the 2BI exhibits more plastic strains than the 2BC models, which shows how the bidirectional load limits the inelastic incursion.

4.3. Hysteretic Behavior of the Connections

The hysteretic response curves of all models analyzed are shown in Figure 14, where the vertical coordinate F is the load applied on the top of the column and the horizontal coordinate is the drift rotation of the system. In general, for all models, a ductile and stable hysteretic behavior without pinching and degradations in the strength and stiffness. However, as the width-to-thickness column ratio increases, degradations in the stiffness and strength are noted for all models. The strength degradation is greater in the 2BI models, and the stiffness degradation is greater in the 2BC models. This difference is associated with the failure model exhibited by each model, where the 2BI slender model was controlled by panel shear yielding and the 2BC by the outer annular stiffener bending yield. Additionally, the difference between the high-ductility and moderate-ductility models is small in terms of strength and stiffness; the large difference was for the high inelastic cycles of load.

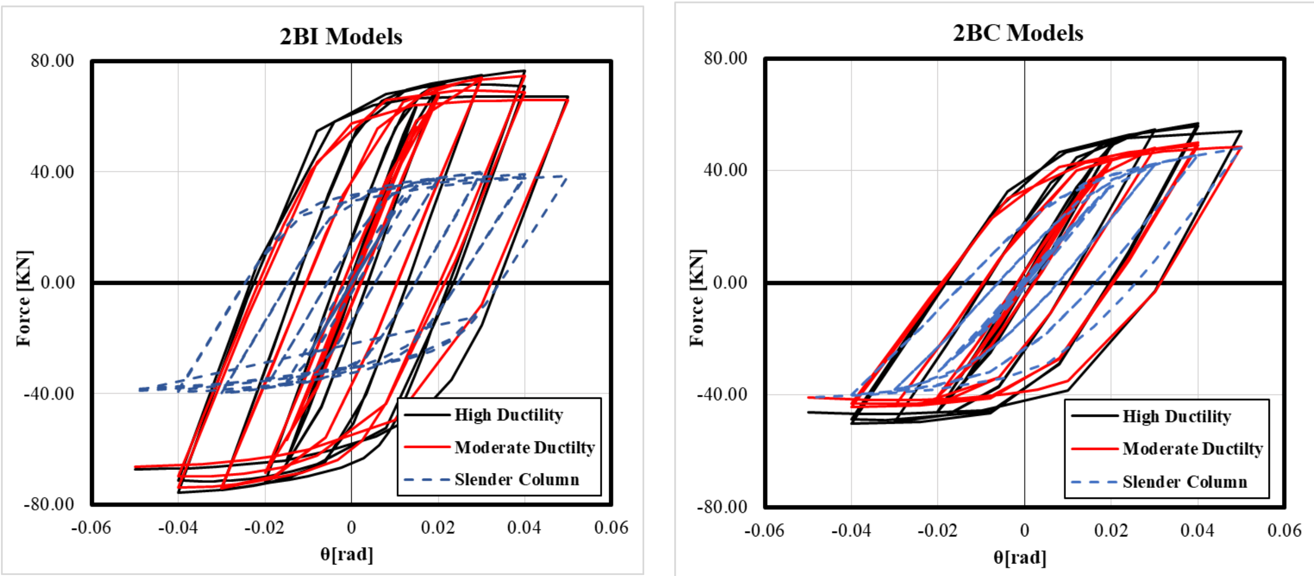

Figure 14. Hysteretic curves for all models analyzed.

A comparison between the 2BI and 2BC models was developed for each width-to-thickness column ratio and is shown in Figure 15. These results indicate that the bidirectional effect causes significant decreases in the strength and stiffness of the joints for the same number of connected beams. Nevertheless, this bidirectional effect had no greater difference between the high-ductility and moderate-ductility models. Furthermore, the slender models continue to show high stiffness degradations when the bidirectional effect is present instead of the strengths being similar. To summarize quantitatively the hysteretic behavior shown previously on hysteretic curves, Table 5 shows the key parameters of the models analyzed.

Table 5. Summary of the parameters obtained in numerical models.

Joint	Width-to-Thickness Ratio	P_{max} (kN)	θ_{max} (rad)	K_o (kN/rad)	$K_{sec\_0.04}$ (kN/rad)	Dissipated Energy (kJ)	ε_{max} (mm/mm)	σ_{max} (MPa)
2BC	High-ductility	56.953	0.05	2718	1423	634	0	255.7
	Moderate-ductility	50.088	0.05	2407	1252	575	0	326.9
	Slender	48.189	0.05	1783	1141	390	0.019	412.2
2BI	High-ductility	76.543	0.05	4572	1913	1118	0	295.1
	Moderate-ductility	74.712	0.05	3935	1867	942	0.007	398
	Slender	39.988	0.05	2580	980	649	0.085	508.3

These results show how stiffness and strength are higher in the models without a bidirectional effect (2BI), even when a slender column is present. In terms of dissipated energy, the difference between the high-ductility and moderate-ductility models is small, in the order of 9%. However, for slender models, the difference between the high-ductility and moderate-ductility models can sustain even a 40% reduction. Additionally, higher dissipated energy is observed for the 2BI slender model in comparison to the 2BC slender model; [8] suggests that shear panel failure is highly ductile and can improve the connection energy dissipation capacity. Moreover, the inelastic incursion of the outer annular stiffeners of the 2BC models is limited, which limits its energy dissipation.

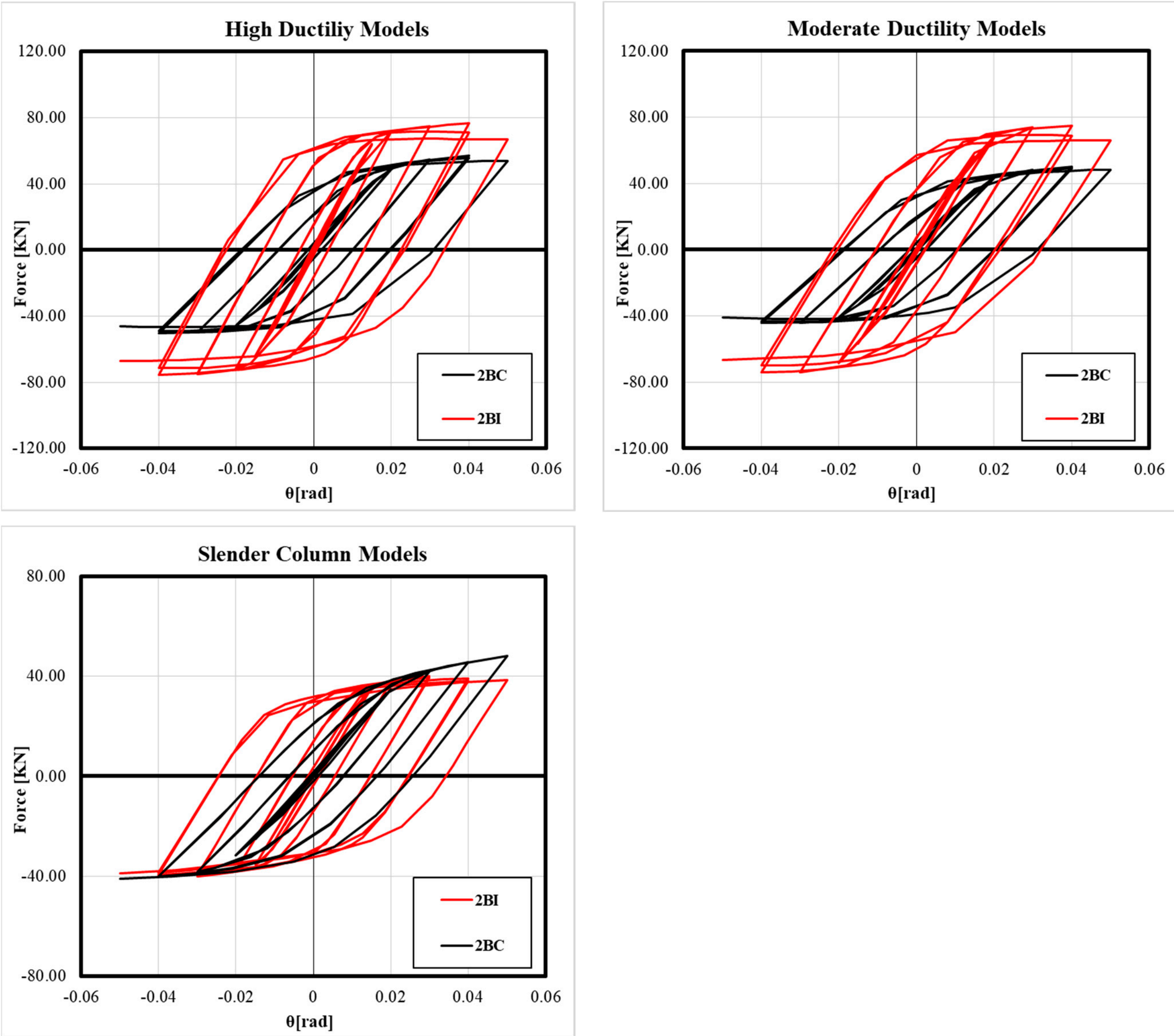

Figure 15. Comparison of the hysteretic curves between joint configurations.

Finally, a high demand in the web panel zone is denoted for interior joints (2BI) and for models with bidirectional effect (2BC) in terms of strain and stress. However, the stability of the system in terms of secant stiffness reduction is higher in 2BC models, in the order of 36%, in comparison to 2BI where the reduction is in the order of 62%.

5. Conclusions

In this research, the assessment of the cyclic behavior of the web panel zone in built-up box columns with different width-to-thickness ratios was performed. An end-plate moment connection proposed by [22] subjected to a bidirectional cyclic loading was used to connect beams to columns. The cyclic response of 3D steel joint configurations was obtained from experimental tests. Moreover, a numerical study using FEM was employed to extend the evaluation to different thicknesses in the panel zone. The effect of bidirectional loading was studied considering the failure mechanism, hysteretic response, stress distribution, strain distribution, energy dissipation capacity, stiffness, and strength of specimens and FE models. Finally, the main conclusions are described as follows:

1. The bidirectional effect reduces the strength and stiffness capacities of the connection; in the absence of the bidirectional effect, the connection can reach 0.8 Mp (plastic moment) and 0.04 rad of rotation as long as the members and components are designed according to the seismic philosophy;
2. High-ductility columns and moderate-ductility columns allow ductile failure mechanisms with plastic hinges in the beams to be reached. Nevertheless, for interior joints, slight plastic deformations could appear without system instability;
3. A combined failure mechanism with plastic hinges in the beams and plastic strains in the web panel zone is achieved for slender web columns. Therefore, the strength and stiffness of the joint configurations decreased;
4. Slender columns reached a the hysteretic behavior of the connection was still ductile until the 0.05 rad rotation. However, a reduction in the energy dissipation capacity occurred until 62% of the original capacity was reached when yielding in shear appeared in the web panel zone;
5. The presence of outer annular stiffeners and vertical stiffeners allows the local buckling on the web panel zone to be avoided, modifying the stress distribution such that is it similar to a diagonal tension field for interior joints and a uniform stress distribution for joints with bidirectional effect. However, these stiffeners should be designed to support the concentrated beam capacity load to transfer the stress properly.

Author Contributions: Conceptualization, E.N.; methodology, E.N. and R.M.; software, R.M. and E.N.; validation, E.N. and F.S.; formal analysis, E.N. and R.M.; investigation, E.N., N.M. and F.S.; resources, N.M. and Á.R.; data curation, E.N.; writing—original draft preparation, E.N. and R.M.; writing—review and editing, E.N. and Á.R.; visualization, E.N.; supervision, E.N.; project administration, E.N.; funding acquisition, Á.R. All authors have read and agreed to the published version of the manuscript.

Funding: This research was funded by Fondecyt N° 11200709 (Agencia Nacional de Investigación y Desarrollo, Chile) and DINNOVA 03/2020-II (UCSC).

Institutional Review Board Statement: Not applicable.

Informed Consent Statement: Not applicable.

Data Availability Statement: Not available.

Acknowledgments: Dirección de postgrado de la UCSC.

Conflicts of Interest: The authors declare no conflict of interest.

References

1. *AISC341-16*; Seismic Provisions for Structural Steel Buildings. American Institute of Steel Construction: Chicago, IL, USA, 2016.
2. *AISC358-16*; Prequalified Connections for Special and Intermediate Steel Moment Frames for Seismic Applications. American Institute of Steel Construction: Chicago, IL, USA, 2016.
3. Krawinkler, H.; Mohasseb, S. Effects of panel zone deformations on seismic response. *J. Constr. Steel Res.* **1987**, *8*, 233–250. [CrossRef]
4. Tuna, M.; Topkaya, C. Panel Zone deformation demands in steel moment resisting frames. *J. Constr. Steel Res.* **2015**, *110*, 65–75. [CrossRef]
5. *ANSI/AISC 360-16*; Specification for Structural Steel Buildings. American Institute of Steel Construction: Chicago, IL, USA, 2016.
6. *FEMA 355D*; State of the Art Report on Connection Performance. Federal Emergency Management Agency: Washington, DC, USA, 2000.
7. *European Standard EN 1993-1-8*; Eurocode 3: Design of Steel structures—Part 1–8: Design of Joints. European Committee for Standardization: Brussels, Belgium, 2005.
8. Skiadopoulos, A.; Lignos, D. Seismic demands of Steel moment resisting frames with inelastic beam-to-column web panel zones. *Earthq. Eng. Struct. Dyn.* **2022**, *51*, 1591–1609. [CrossRef]
9. Adlparvar, M.R.; Vetr, M.G.; Ghaffari, F. The importance of panel zone shear strength on seismic behavior of improved slotted-web beam connection. *Int. J. Steel Struct.* **2017**, *17*, 307–318. [CrossRef]
10. Hanna, M.T. Failure Loads of web panels loaded in pure shear. *J. Constr. Steel Res.* **2015**, *105*, 39–48. [CrossRef]
11. Brandonisio, G.; de Luca, A.; Mele, E. Shear inestability of panel zone in beam-to-column connections. *J. Constr. Steel Res.* **2011**, *67*, 891–903. [CrossRef]

12. Augusto, H.; da Silva, L.S.; Rebelo, C.; Castro, J. Characterization of web panel components in double-extended bolted end-plate steel joints. *J. Constr. Steel Res.* **2016**, *116*, 271–903. [CrossRef]
13. Choi, Y.S.; Kim, D.; Lee, S.C. Ultimate Shear behavior of web panels of HSB800 plate griders. *Constr. Build. Mater.* **2015**, *101*, 828–837. [CrossRef]
14. Leblouba, M.; Barakat, S.; Al-Saadon, Z. Shear Behavior of corrugated web panels and sensitivity analysis. *J. Constr. Steel Res.* **2018**, *151*, 94–107. [CrossRef]
15. Lee, S.; Lee, D.; Yoo, C. Design of intermediate transverse stiffeners for shear web panels. *Eng. Struct.* **2014**, *75*, 27–38. [CrossRef]
16. Pan, L.; Chen, Y.; Chuan, G.; Jiao, W.; Xu, T. Experimental evaluation of the effect of vertical connecting plates on panel zone shear stability. *Thin-Walled Struct.* **2016**, *99*, 119–131. [CrossRef]
17. Xu, Y.; Hao, J. Seismic performance of spatial beam-column connections in steel frame. *J. Constr. Steel Res.* **2021**, *180*, 106586. [CrossRef]
18. Fadden, M.; McCormik, J. HSS-to-HSS seismic moment connection performance and design. *J. Constr. Steel Res.* **2014**, *101*, 373–384. [CrossRef]
19. Nia, Z.S.; Ghassemieh, M.; Mazroi, A. WUF-W connection performance to box column subjected to uniaxial and biaxial loading. *J. Constr. Steel Res.* **2013**, *88*, 90–108.
20. Chen, X.; Shi, G. Experimental study of end-plate joints with box columns. *J. Constr. Steel Res.* **2018**, *143*, 307–319. [CrossRef]
21. Mohammadi, S.; Ghassemieh, M.; Mirghaderi, S.R. Cyclic behavior of steel moment connections with built-up columns in weak direction. *J. Constr. Steel Res.* **2020**, *172*, 106224. [CrossRef]
22. Nuñez, E.; Torres, R.; Herrera, R. Seismic performance of moment connections in steel moment frames with HSS columns. *Steel Comp. Struct.* **2017**, *25*, 271–286.
23. Bai, Y.; Wang, S.; Mou, B.; Wang, Y.; Skalomenos, K. Bi-directional seismic behavior of steel beam-column connections with outer annular stiffener. *Eng. Struct.* **2021**, *227*, 111443. [CrossRef]
24. Qin, Y.; Chen, Z.; Yang, Q.; Shang, K. Experimental seismic behavior of through diaphragm connections to concrete-filled rectangular steel tubular columns. *J. Constr. Steel Res.* **2014**, *93*, 32–43. [CrossRef]
25. Nia, Z.S.; Ghassemieh, M.; Mazroi, A. Panel zone evaluation of direct connection to box column subjected to bidirectional loading. *Struct. Des. Tall Spec. Build.* **2014**, *23*, 833–853.
26. Sarfarazi, S. Evaluation of panel zone shear strength in cruciform columns, box-columns and double web-columns. *Int. J. Struct. Civ. Eng.* **2016**, *5*, 52–56. [CrossRef]
27. Pazmiño, C.; Moscoso, M.; Arévalo, D.; Guaminga, E.; Gómez, C.; Herrera, M.; Vintimilla, J. Experimental study of Steel tube panel under in-plane lateral cyclic load. *Case Stud. Constr. Mater.* **2019**, *11*, e00270. [CrossRef]
28. Rong, B.; Liu, S.; Yan, J.; Zhang, R. Shear Behavior of panel zone in through-diaphragm connections to steel tubular columns. *Thin-Walled Struct.* **2018**, *122*, 286–299. [CrossRef]
29. Gallegos, M.; Nuñez, E.; Herrera, R. Numerical study on cyclic response of end-plate biaxial moment connection in box columns. *Metals* **2020**, *10*, 523. [CrossRef]
30. Nuñez, E.; Lichtemberg, R.; Herrera, R. Cyclic performance of end-plate biaxial moment connection with HSS columns. *Metals* **2020**, *10*, 1556. [CrossRef]
31. Mata, R.; Nuñez, E. Parametric study of 3D steel moment connections with built-up box column subjected to biaxial cyclic loads. *J. Constr. Steel Res.* **2022**, *197*, 107453. [CrossRef]
32. ANSYS, Inc. *Theory Reference for ANSYS and ANSYS Workbench Release 19.0*; ANSYS, Inc.: Canonsburg, PA, USA, 2019.
33. Moura, P.; Carvalho, H.; Figueiredo, L.; Aires, P.; Bártolo, R. Unitary model for the analysis of bolted connections using the finite element method. *Eng. Fail. Anal.* **2019**, *104*, 308–320.
34. Amadio, C.; Bedon, C.; Fasan, M.; Pecce, M. Refined numerical modelling for the structural assessment of steel-concrete composite beam-to-column joints under seismic loads. *Eng. Struct.* **2017**, *138*, 394–409. [CrossRef]
35. *ASTM-A6/A6M*; Standard Specification for General Requirements for Rolled Structural Steel Bars, Plates, Shapes, and Sheet Piling. ASTM: West Conshohocken, PA, USA, 2011.
36. *ASTM-A500/A500M*; Standard Specification for Cold-Formed Welded and Seamless Carbon Steel Structural Tubing in Rounds and Shapes. ASTM: West Conshohocken, PA, USA, 2021.
37. Tartaglia, R.; D'Aniello, M.; Rassati, G.A.; Swanson, J.A.; Landolfo, R. Full strength extended stiffened end-plate joints: AISC vs recent European design criteria. *Eng. Struct.* **2018**, *159*, 155–171. [CrossRef]